ANL/NSE-21/74

FY21 SAM Developments for MSR Modeling

Nuclear Science and Engineering Division

ANL/NSE-21/74

FY21 SAM Developments for MSR Modeling

prepared by
R. Hu, G. Hu, M. Gorman, J. Fang, T. Mui, D. O'Grady, T. Fei
Nuclear Science and Engineering Division, Argonne National Laboratory

R. Salko
Oak Ridge National Laboratory

September 2021

ABSTRACT

An advanced system analysis tool, SAM, is under development for advanced non-LWR reactor safety analysis, including molten salt reactors (MSR). To support the development and utilization of the SAM code for MSR safety analysis and licensing, continuous efforts have been devoted to enhancing code capabilities and updating reference models for the MSRs. This report documents the FY21 progress in SAM code development, capability enhancements, and reference model development to support transient safety analysis of MSRs, including code enhancements in reactor kinetics and reactivity feedback modeling for liquid fuel reactors, updates of the Molten Salt Reactor Experiment (MSRE) primary system model, developments and updates of the molten salt fast reactor (MSFR) model based on EVOL design, and implementation of a drift flux model for modeling gas transport in MSR systems.

Table of Contents

LIST OF FIGURES

LIST OF TABLES

1 Introduction

An advanced system analysis tool, SAM, is under development for advanced non-LWR reactor safety analysis (Hu et al. 2021), supported by DOE-NE's Nuclear Energy Advanced Modeling and Simulation (NEAMS) program. It aims to provide fast-running, modest-fidelity, whole-plant transient analyses capabilities, which are essential for fast turnaround design scoping and engineering analyses of advanced reactor concepts. SAM aims to be a generic system-level safety analysis tool for advanced non-LWRs, including liquid-metal-cooled fast reactors (LMFR), molten salt reactors (MSR), fluoride-salt-cooled high-temperature reactors (FHR), and high-temperature gas-cooled reactors (HTGR). It takes advantage of advances in physical modeling, numerical methods, and software engineering to enhance its user experience and usability.

In recently years, there is a renewed interest in MSR technology in the development of future advanced nuclear reactors. To support the development and utilization of the SAM code for MSR safety analysis and licensing, continuous efforts have been devoted to enhancing code capabilities and updating reference models for the MSR primary loop. A reference standard problem of a prototypical reactor design is foundational to nuclear industry and regulators to verify the adequacy of computer codes and evaluation models for a specific reactor type.

This report documents the FY21 progress in SAM code development, capability enhancements, and reference model development to support transient safety analysis of MSRs. This report is structured as follows: Section 2 provides a summary on SAM code enhancements in reactor kinetics and reactivity feedback modeling for liquid fuel reactors. Section 3 discusses the model updates of the Molten Salt Reactor Experiment (MSRE) primary system using SAM. Section 4 describes SAM model developments and updates of the molten salt fast reactor (MSFR) based on EVOL design. Section 5 describes improvements in modeling gas transport in MSR systems based on a newly implemented drift flux model.

2 Enhancements for Reactivity Feedback Modeling

In FY21, the SAM point kinetics equation and reactivity feedback models are enhanced to improve SAM's capabilities in modeling and simulations of MSRs. Several of major enhancements are listed and explained below:

- Flexibility in defining core inlet and outlet
- Add moving fuel Doppler reactivity feedback model
- Add moderator reactivity feedback model
- Update of fuel axial expansion reactivity feedback model for liquid fuel
- Update of fuel Doppler reactivity feedback coefficients

2.1 Flexibility in defining core inlet and outlet

The current SAM point kinetic equation is implemented as Equation 2-1 combined with Equation 2-2 and 2-3. c_i is the number of delayed neutron precursor per kg of fuel, and C_i is the total population of the precursors in the channels with precursor source.

$$\frac{\mathrm{dn}}{\mathrm{dt}} = \frac{\rho - \beta - \sum_i \left(\dot{c}_{in,i}(0) - \dot{c}_{out,i}(0)\right)\Lambda}{\Lambda} n + \sum_i \lambda_i C_i \,, \tag{2-1}$$

$$\frac{\mathrm{dC_i}}{\mathrm{dt}} = \frac{\beta_i}{\Lambda} n - \lambda_i C_i + \left(\dot{c}_{in,i} - \dot{c}_{out,i}\right). \tag{2-2}$$

$$\frac{\partial \rho c_i}{\partial t} + \frac{u \partial \rho c_i}{\partial x} = \frac{\beta_i}{\Lambda} n - \lambda_i \rho c_i \tag{2-3}$$

Equation 2-3 is solved simultaneously with the system flow equation to provide the distribution of precursors density in fluid channels. It should be noted that Equation 2-2 is essentially the integration of Equation 2-3 in all channels with precursor source. Solving Equation 2-2 can be completely avoided by integrating c_i along the channels with precursor source as depicted in Equation 2-4.

$$C_i(t) = \sum_{j(\#\ channels)} \int \rho(x,t) c_{i,j}(x,t) dx \tag{2-4}$$

This modification should have little impact on the results theoretically and has been implemented into SAM in FY2.

The moving fuel of MSR is not bounded by a well-defined reactor core, in contrast to solid fuel types of reactors. The definition of core inlet and outlet boundary is important for evaluation of reactivity from delay neutron precursor. In FY21, the SAM point kinetic equation implementation was further modified to separate the precursor source, flowing-in, flowing-out, and integration channels. This allows more flexibility of using the point kinetic model in SAM. It also removes redundant postprocessors for the flowing-in and flowing-out precursor terms ($\dot{c}_{in,i}(0) - \dot{c}_{out,i}(0)$ term in Equation 2-1). The $\dot{c}_{in,i}$ and $\dot{c}_{out,i}$will be calculated for the flowing-in channels and flowing-out channels, respectively. $C_i(t)$ will only be calculated by integrating the precursor concentrations in the integration channels. An example of the modified input is presented

in Figure 2-1. In this example, the flowing-in and flowing-out terms are calculated for Channel *ch2*. The precursor population $C_i(t)$ is calculated by integrating the precursor concentration along Channel *ch2*. However, the precursor source is specified in both Channel *ch2* and *uplnm*.

```
constant_power                = True
Moving_DNP_bypass_channels    = 'ch2 uplnm'
feedback_components           = 'ch2 moderator'
flowing_in_DNP_channels       = 'ch2'
flowing_out_DNP_channels      = 'ch2'
integrate_DNP_channels        = 'ch2'
```

Figure 2-1 An example input for modified SAM code.

2.2 Moving fuel Doppler reactivity feedbacks

In the previous SAM implementations, the fuel Doppler reactivity feedback model was designed for application of solid fuel (e.g. pin-type or pebble-type solid fuel) and was not supposed to be used for moving fuel, as in MSR. In the previous modeling practice, the moving fuel reactivity was modeled using the coolant density reactivity feedback model. This caused difficulties in preparing the appropriate reactivity feedback coefficients, because fuel Doppler and coolant density reactivity feedbacks are different in nature.

Therefore, the fuel Doppler reactivity feedback model for a MSR channel is added in FY21 with a model similar to solid fuel, but using the moving fuel temperature as the reference. For a MSR channel divided into N layers, the liquid fuel Doppler reactivity feedback is modeled by,

$$R_D(t) = \sum_n^N \alpha_D^n \times \ln\left[T_f^n(t) \,/\, T_f^n(0)\right] \qquad (2\text{-}5)$$

where α_D^n is the fuel Doppler reactivity coefficient of layer n in unit of $\Delta k/k$ per $ln((T + \Delta T)/T)$, $T_f^n(t)$ is the transient average fuel temperature and $T_f^n(0)$ is the average fuel temperature at the start of the transient.

2.3 Moderator reactivity feedback model

The moderator thermal reactivity feedback is modeled in the *HeatStructure* component using the layered average solid temperature. Suppose the solid structure (e.g. graphite) is divided into N axial layers, the thermal reactivity feedback from this solid structure is modeled by,

$$R_M(t) = \sum_n^N \alpha_M^n \times \left[T_f^n(t) - T_f^n(0)\right] \qquad (2\text{-}6)$$

where α_M^n is the moderator reactivity coefficient of layer n in unit of $\Delta k/k$ per K, $T_f^n(t)$ is the transient average solid temperature, and $T_f^n(0)$ is the average solid temperature at the start of the transient.

2.4 Update of fuel axial expansion reactivity feedback model

In SAM, the fuel axial expansion model was developed to consider the reactivity feedback in response to the fuel temperature changes and fuel expansion during the transient. The fuel axial expansion reactivity is calculated by the difference between the transient and initial values of total reactivity worth in the fuel pins,

$$R_{\mathrm{A}}(t) = \int_{z=0}^{z=L'} \rho_f(\xi, t) \times f(\xi) \times A \, d\xi$$
$$\Delta R_{\mathrm{A}}(t) = R_{\mathrm{A}}(t) - R_{\mathrm{A}}^{ss} \qquad (2\text{-}7)$$

where ΔR_{A} is the fuel axial expansion reactivity feedback in the unit of Δk/k; $\rho_f(\xi, t)$ is the fuel density at transient time t in the unit of kg/m^3; $f(\xi)$ is the fuel reactivity coefficient in unit of *Δk/k / kg*; L' and A are the expanded fuel length during the transient and cross-section area, respectively. The integration will consider the axial thermal expansion of the fuel pin.

The fuel axial expansion reactivity model was implemented in SAM using the linear thermal expansion coefficient of fuel and cladding material, which are used in estimating the fuel pin axial displacement due to the temperature change. This model and the implementation work well for the solid fuel where the axial expansion is small. However, this model faces some issues in case of liquid fuel:

- The assumption of linear thermal expansion was valid for solid fuel where the thermal expansion is relatively small. However, this assumption becomes problematic in case of liquid fuel, such as used in molten-salt reactor, where the axial thermal expansion (and fuel density change) could be significant. The fuel density changes nonlinearly with fuel temperature.
- During the transient, there could be a portion of fuel outside the nominal fuel length due to the thermal expansion. The exact reactivity worth of this portion of fuel needs being provided by the reactor physics calculation. In the SAM implementation, the value of fuel reactivity function (f) beyond the nominal fuel length represents this effect. This is understood as an input that should be provided by the SAM users. In practice, this information could be difficult to obtain. In the case of solid fuel, because the thermal expansion is small, the effect of this portion of fuel is minimal and can be safely ignored. However, this is not the case for liquid fuel.

To overcome these issues, a new fuel axial expansion reactivity feedback model is added into SAM for better treatment of liquid fuel. In this new model, the density change of the fuel during the transient is directly used in estimating the reactivity. Let the mesh size be Δz. Let f_i and ρ_i be the reactivity worth and fuel density at the i-th layer. The fuel axial expansion reactivity inside the fixed mesh (i.e. the nominal fuel length region) is evaluated with

$$\Delta R' = \sum_{i=1}^{N} [\rho_i(t) - \rho_i^{\mathrm{ss}}] \, f_i A \Delta z \qquad (2\text{-}8)$$

where ρ_i is temperature dependent during the transient. The reactivity contribution of the fuel beyond the fixed mesh is considered by

$$\Delta R^* = f^* \rho_N(t) A[L' - L] \quad (2\text{-}9)$$

where f^* is the value of fuel reactivity function beyond the fixed mesh, $\rho_N(t)$ is the density of the last layer of fuel, and L' is the expanded fuel length during the transient. L' is calculated from the fuel density change using mass conservation. The total fuel axial expansion reactivity is

$$\Delta R_{\mathrm{A}}(t) = \Delta R' + \Delta R^* = \sum_{i=1}^{N} [\rho_i(t) - \rho_i^{\mathrm{ss}}] f_i A \Delta z + f^* \rho_N(t) A[L'(t) - L] \quad (2\text{-}10)$$

This new model avoids the assumption of linear thermal expansion by using directly the fuel density change with fuel temperature and is thus valid for liquid fuel, and considers the reactivity contribution from the fuel expanded outside the nominal fuel length. Numerical verification tests showed that it worked very well for liquid fuel. This update is particularly important for the stable salt reactor concept which use liquid fuel inside a fuel pin.

2.5 Update of fuel Doppler reactivity feedback coefficients

The current reactivity feedback mechanisms within SAM allow for two kinds of direct temperature feedback, Fuel Doppler and Moderator feedback. Fuel Doppler feedback assumes that the partial derivative of reactivity with respect to temperature is

$$\frac{\partial \rho}{\partial T}_D = \frac{\alpha_D}{T} \quad (2\text{-}11)$$

where α_D is the Doppler feedback coefficient, ρ is the reactivity of the core and T is the temperature of the fuel. Moderator feedback assumes that the partial derivative of reactivity with respect to temperature is

$$\frac{\partial \rho}{\partial T}_M = \alpha_M \quad (2\text{-}12)$$

where α_M is the moderator feedback coefficient, and T is the temperature of the moderator.

Both temperature feedbacks attempt to capture the Doppler broadening that occurs within the absorption cross section due to a change in material temperature. The temperature dependence of the broadening is a function of the spectrum. In thermal reactors, the impact of Doppler broadening can be capture using

$$\frac{\partial \rho}{\partial T} = \alpha \quad (2\text{-}13)$$

however, it has been observed that some light water reactors show a fuel temperature dependence that is better described using

$$\frac{\partial \rho}{\partial T} = \frac{\alpha}{\sqrt{T}} \quad (2\text{-}14)$$

In fast reactors, the impact of Doppler broadening can be captured using

$$\frac{\partial \rho}{\partial T} = \frac{\alpha}{T} \tag{2-15}$$

however, it has been observed that some of the fast reactors show a slight deviation from the $1/T$ behavior and are better described using a more general form

$$\frac{\partial \rho}{\partial T} = \alpha T^{-n} \tag{2-16}$$

where n can range from 0.8 to 1.2.

In order to improve the applicability of SAM for fast, thermal and epi-thermal reactors, the temperature reactivity feedbacks should be updated to allow for a flexible temperature reactivity formulation

$$\frac{\partial \rho}{\partial T} = \alpha T^{-n} \tag{2-17}$$

where α is the temperature feedback coefficient, T is the temperature of the material and n is a user supplied constant. The resulting change in reactivity will be calculated using

$$\rho_2 - \rho_1 = \begin{cases} \alpha(T_2^{-n+1} - T_1^{-n+1}) & if\ n \neq 1 \\ \alpha \ln\left(\frac{T_2}{T_1}\right) & if\ n = 1 \end{cases} \tag{2-18}$$

3 Updated Primary Loop Model of MSRE

The MSRE was a graphite moderated flowing salt type reactor with a design maximum operating power of 10 MW(th) (Robertson, 1965). The fuel salt was a mixture of lithium, beryllium, and zirconium fluoride containing uranium or thorium and uranium fluoride. The coolant salt was a mixture of lithium fluoride and beryllium fluoride. The reactor consisted of two flow loops: a primary loop and a secondary loop. The primary loop connected the reactor vessel to a fuel salt centrifugal pump and the shell side of the shell-and-tube heat exchanger. The secondary loop connected the tube-side of the shell-and-tube heat exchanger to a coolant salt centrifugal pump and the tube side of an air-cooled radiator. Two axial blowers supplied cooling air to the radiator. Piping, drain tanks and "freeze valves" made up the remaining components of the heat transport circuits. The heat generated in the core was transferred to the secondary loop through the heat exchanger and ultimately rejected to the atmosphere through the radiator. Here we focused on the modeling of the MSRE primary loop. A coupled 2-D/1-D MSRE model has been previously reported (Fang et al., 2020) with a porous medium modeling of the core region, based on which the current study developed a light-weighted 1-D model of the entire primary loop including the core. While the coupled 2-D/1-D MSRE model may provide more accurate modeling inside the core region, it is also more computationally demanding compared to the 1-D model. The 1-D model would be more suitable for scenarios where quick turnaround time is preferred, and thus motivated this follow-up development. This model update is also being used in the MSRE benchmark simulation pursued under the NEAMS MSR Application Driver efforts.

3.1 Model setups and material properties

As illustrated in Figure 3-1, the main components in the MSRE primary loop are a reactor core including the lower and upper plenum, a pump, a primary heat exchanger, and all the connecting pipes involved. A system reference pressure boundary condition is applied to the exit of heat exchanger at the primary side to aid faster convergence and robustness of the SAM simulations. The overall layout shown in Figure 3-1 resembles that of the original MSRE designs(Beall et al., 1964). The fuel salt in the primary loop was LiF-BeF_4-ZrF_4-UF_4 according to the design specifications of the MSRE (Beall et al., 1964; Cantor, 1968), of which the thermophysical properties are listed in Table 3-1. The related correlations are employed in the customized EOS in the SAM input file. A total power of 10 MW is considered in the core, which is uniformly deposited along the axial direction.

Table 3-1. Thermophysical properties of the fuel salt.

		Unit	LiF-BeF_4-ZrF_4-UF_4
Melting temperature	T_{melt}	K	722.15
Density	ρ	kg/m^3	$2553.3 - 0.562 \cdot T$
Dynamic viscosity	μ	Pa·s	$8.4 \times 10^{-5} \exp(4340/T)$
Thermal conductivity	k	W/(m·K)	1.0
Specific heat capacity	c_p	J/(kg·K)	2009.66

A conventional, cross-baffled, shell-and-tube type heat exchanger was used in MSRE. The fuel salt flows on the shell side while the coolant salt flows through the tube side. The coolant salt in the heat changer is LiF-BeF2 (0.66-0.34) (Guymon, 1973), of which the major thermophysical properties are summarized in Table 3-2. Due to the space limitation in the reactor cell, a U-tube configuration is adopted, which results in a heat exchanger of roughly 2.5 m in length. The shell

diameter is 0.41 m while the tube has a diameter of 1.27 cm and a thickness of 1.07 mm. Given a triangular arrangement of the heat exchanger tubes, the hydraulic diameters are estimated to be 2.09 cm (shell-side) and 1.06 cm (tube-side). The construction material of heat exchanger is Hastelloy® N alloy with the properties listed in Table 3-3. All the connecting pipes have a default diameter of 0.127 m. A centrifugal pump is utilized, and its head is adjusted to sustain the flow circulation. The downcomer, lower plenum, and the upper plenum are all modeled with the SAM 1-D components with various discretization resolutions.

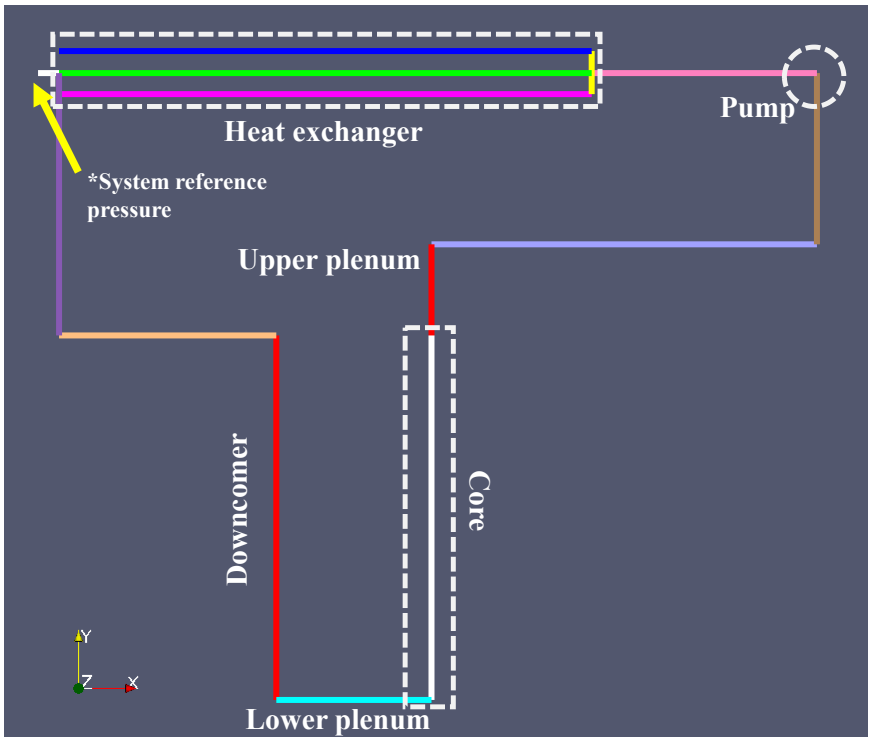

Figure 3-1. The structure of MSRE primary loop represented.

Table 3-2. Thermophysical properties of the coolant salt in heat exchanger.

		Unit	$LiF\text{-}BeF_2$ (0.66-0.34)
Melting temperature	T_{melt}	K	728
Density	ρ	kg/m^3	$2146.3 - 0.4884 \cdot T$
Dynamic viscosity	μ	Pa·s	$1.16 \times 10^{-4} \exp(3755/T)$
Thermal conductivity	k	W/(m·K)	1.1
Specific heat capacity	c_p	J/(kg·K)	2390

Table 3-3. Thermophysical properties of Hastelloy® N alloy.

		Unit	Hastelloy® N alloy
Density	ρ	kg/m^3	8860
Thermal conductivity	k	W/(m·K)	23.6
Specific heat	c_p	J/(kg·K)	578

3.2 Results

Figure 3-2 shows the steady state fuel salt temperature in the primary loop during the normal operating condition. The fuel salt enters the MSRE core at an average temperature of 908K, and through the heat transfer in the core region, leaves the core at an average temperature of 937K. The overall temperature distribution is consistent with that observed in our previous coupled 2-D/1-D model. The primary pump is located at the top-right corner, driving the fuel salt in the system. The U-tube primary heat exchanger cools down the fuel salt, which returns to the core through the connecting pipes, downcomer and the core inlet plenum. Though the current 1-D model works well, it is still a significant simplification to model the core region with only one 1-D channel, and the simulation can be further improved by using multiple 1-D channels to represent the core.

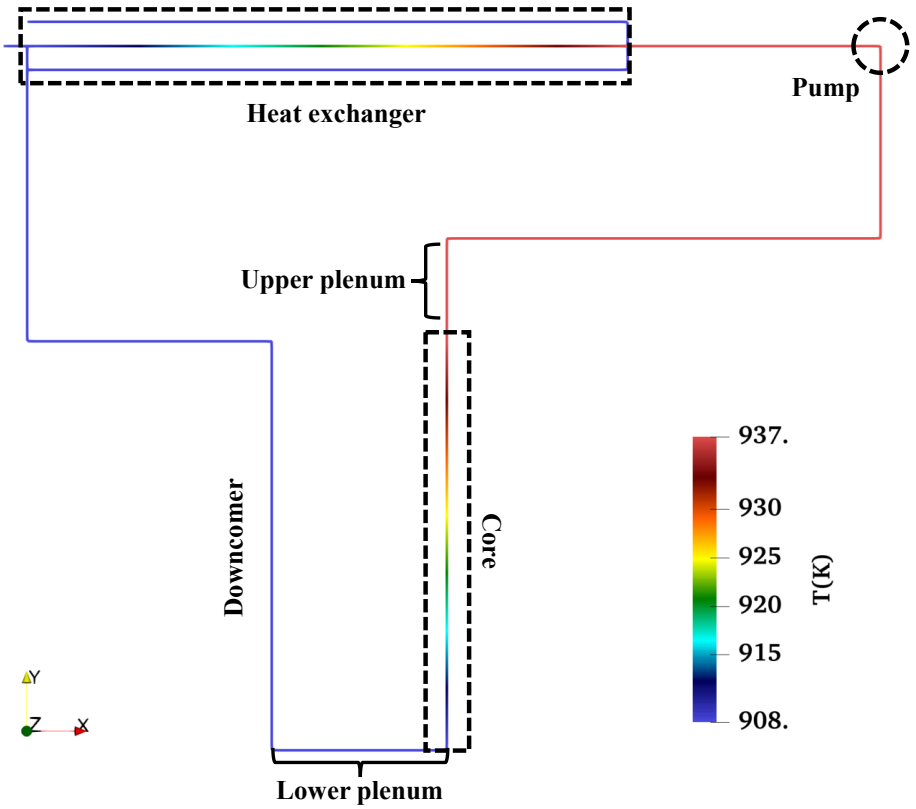

Figure 3-2. The steady-state temperature distribution in the 1-D loop.

4 Model Improvements and Demonstration Simulation of MSFR

Recent code developments in the System Analysis Module (SAM) code have been made to further the code capabilities for modelling molten salt reactors (MSRs), including the capability of modeling multi-dimensional components, multi-dimensional species transport, and the capability to model the reactor transients of these multi-dimensional components using the point kinetics equations (PKEs). When used together, SAM can model a MSR system where the reactor core is modeled in 2D/3D with species transport to track fission products, such as delayed neutron precursors (DNPs), and predict reactor transients using the modified PKEs while the rest of the system (i.e. pipes, pumps, IHX) can be modeled as a traditional 1D system code.

To demonstrate the current code development efforts, the coupled 2D-1D Molten Salt Fast Reactor (MSFR) model (Fang et al. 2020) was utilized, and simulations were performed under steady state and prescribed transient conditions. A standalone 1D model, which acts as a traditional system code approach, was also developed to provide a baseline model for comparison. The 2D-1D coupled and standalone 1D models were developed based on the EVOL MSFR design (Rouch 2014). This work also laid the foundation for the coupled SAM-Pronghorn (planned in FY22) and coupled SAM-Pronghorn-Griffin model development, for a reference MSR design.

4.1 EVOL MSFR

The EVOL MSFR is a 16-loop 3000 MW reactor which uses a lithium fluoride and thorium fluoride salt mixture in the primary fuel circuit. The fuel circuit of the EVOL MSFR includes the core region, core inlet and outlet piping, a separation and reprocessing system, pumps, heat exchangers, and a bubble injection system. The fuel salt circulates from the bottom of the core to the top and has a typical recirculation time of around 3-4 seconds. The MSFR core region is surrounded by a fertile blanket which is used to increase the breeding ratio, and the core also has reflector regions located at the top and bottom of the core cavity. The EVOL MSFR provides advantages over a typical thermal molten salt reactor by removing the need of graphite moderators within the core and having a higher breeding ratio. The system characteristics of the EVOL MSFR design are shown below in Table 4-1.

Table 4-1. Proposed system characteristics of the EVOL MSFR.

Parameter	Value
Reactor Power	3000 MW
Total Mass Flow	~18,900 kg/s
Core Inlet/Outlet Temps.	~900 K / 1000 K
System Pressure	~1 bar
Number of Primary Loops	16
Mass Flow per Loop	~1180 kg/s
IHX Secondary Side Inlet/Outlet Temps.	~863 K / 893 K
IHX Secondary Side Velocity	2.86 m/s
Primary Salt	$LiF\text{-}ThF_4$
Secondary Salt	$LiF\text{-}BeF_2$ (FLiBe)

4.2 Model Methodology

Both the coupled 2D-1D model and standalone 1D model were developed based on the specific MSFR design found in Rouch et al. (2014) which includes fuel salt thermophysical properties, power distribution profiles, core operating conditions, and proposed core geometries. Thermophysical properties of the primary fuel salt used in the simulations are summarized below in Table 4-2 (Pettersen 2016).

Table 4-2. Thermophysical properties of the primary fuel salt (LiF-ThF_4).

Parameter		Units	Value
Density	ρ	$\frac{kg}{m^3}$	$4983.56 - 0.882(T)$
Specific Heat Capacity	c_p	$\frac{J}{kg \cdot K}$	$-1111 + 2.78(T)$
Thermal Conductivity	k	$\frac{W}{m \cdot K}$	$0.928 + 8.4 \cdot 10^{-5}(T)$
Dynamic Viscosity	μ	$Pa \cdot s$	$\rho \cdot (5.54 \cdot 10^{-8}) \cdot \exp\left(\frac{3689}{T}\right)$

Species transport for tracking DNP drift through the system was also implemented in both the coupled 2D-1D model and the standalone 1D model. The species transport equation used in SAM is shown below in Eq. 3-1.

$$\frac{\partial \rho c_i}{\partial t} + \nabla \cdot (\rho \vec{v} c_i) - \nabla \cdot (\mathrm{D_i} \nabla \mathrm{c_i}) + \lambda_\mathrm{i} \rho \mathrm{c_i} = S_i \tag{3-1}$$

Where c_i is the species concentration of precursor type i, ρ is the fuel salt density, $\vec{v}$ is the fuel salt velocity, D_i is the diffusion coefficient of precursor type i, λ_i is the decay constant of precursor type i, and S_i is the source term for precursor type i. Species properties used for transport and PKE calculations are based on the 6-group DNP model.

For predicting the transient reactor power, SAM has developed a set of modified PKEs which accounts for the reactivity feedback from DNP drift in the reactor core. The modified set of PKEs used in SAM is shown below in Eq. 3-2 and 3-3.

$$\frac{dP(t)}{dt} = \frac{\rho - \beta_{eff} - \sum_i (\dot{c}_{in,i}(0) - \dot{c}_{out,i}(0))\Lambda}{\Lambda} P(t) + \sum \lambda_i c_i(t) \tag{3-2}$$

$$\frac{dc_i}{dt} = \frac{\beta_i}{\Lambda} P(t) - \lambda_i c_i + \left(\dot{c}_{in,i} - \dot{c}_{out,i}\right) \tag{3-3}$$

Where P is the reactor power, ρ is the external reactivity effects, β_{eff} is the effective delayed neutron fraction, Λ is the mean neutron generation time, $\dot{c}_{in,i}$ is the core inlet species flux of

precursor type i, $\dot{c}_{out,i}$ is the core outlet species flux of precursor type i, and lastly, λ_i and c_i are the same as they are defined above. Reactivity feedback for fuel density and doppler effects were also included in both models. The reactivity feedback was calculated based on the average fuel salt temperature, and feedback coefficients used were taken from SERPENT calculations performed at the Paul Scherrer Institute of the same MSFR design (Pettersen 2016).

4.2.1 Coupled 2D-1D Model

The coupled 2D-1D model was developed where the core region and core inlet and outlet pipes were modeled in the 2D domain while the rest of the system (i.e. IHXs, pumps, connecting pipes) were modeled as traditional 1D system components. The 2D domain was modeled axisymmetric in RZ coordinates about the center of the core. As mentioned previously, the core geometry was modeled based on a preliminary study by Rouch et al. (2014) which modified the core cavity to improve flow distribution and reduce temperature hot spots in the upper core cavity.

The core outlet boundary is coupled to the 1D system such that the side average values of pressure, velocity, and temperature provide the inlet condition for the 1D system. Similarly, the outlet conditions of pressure, velocity, and temperature in the 1D system are transferred to the 2D core inlet domain as boundary conditions. No-slip conditions are applied to the core walls, and the core centerline serves as the axis of symmetry.

The power distribution in the MSFR core was assumed to be a 2D cosine shape with respect to the radial distance from the center of the core and the axial elevation from the center of the core. The power distribution profile was used for both the volumetric heat generation rate in the core and as the source term for species transport of the DNPs. The equation used to model the power distribution in the core is shown below in Eq. 3-4.

$$q''' = (5.03678 \cdot 10^8) \cdot cos\left(\frac{\pi}{2} \cdot \frac{r}{r_0}\right) \cdot cos\left(\frac{\pi}{2} \cdot \frac{y}{y_0}\right) \left[\frac{W}{m^3}\right] \quad (3\text{-}4)$$

Where r is the radial distance from the center of the core, r_0 is the extrapolated core radius, y is the axial distance from the center of the core, and y_0 is the extrapolated core axial distance. For the simulations performed, values for r_0 and y_0 were 2.55 m and 1.33 m, respectfully. The power density profile was integrated over the domain to verify the total power was correct.

4.2.2 Standalone 1D Model

The standalone 1D model was developed to model the EVOL MSFR as a traditional 1D system code approach. The model consists of 2 loops composing of 1D components built into the SAM code. For the model, a *PBMoltenSaltChannel* was used to model the MSFR core, *PBOneDFluidComponents* were used to model the core piping and other connecting pipes, *PBHeatExchangers* were used to model the IHXs, and *PBPumps* were used model the pumps in the system. The system was designed and modified to best match the design characteristics shown in Table 4-1, but considerations were also taken to try and match characteristics found in the coupled 2D-1D loop for a better comparison between the two models.

4.3 Results and Discussion

Steady state and transient simulations were performed for both the coupled 2D-1D model and the standalone 1D model. The steady state models were tuned to best match the design characteristics of the EVOL MSFR shown in Table 4-1. The limiting factor for reaching steady state in both models was found to be the circulation of DNP group 1 because of the long half-life (~80s) of the precursor. Nominal operating conditions were observed, and the steady state results were also used to initialize the transient simulations. The transient scenario simulated involved a pump coast-down effect on the MSFR system. The pump coast-down transient was initiated at $t = 1$ s into the simulation, and then the pump head was reduced to 20% of the nominal pump head over a time interval of 10 seconds. The pump was then maintained at 20% of the nominal head, and the simulation continued until the system reached a new steady state condition. Results between the coupled 2D-1D model and the standalone 1D model were analyzed and compared for steady state and transient conditions.

The species concentrations in the standalone 1D model were seen to follow similar behavior as what was found in the coupled 2D-1D model. Specifically, the long-lived DNP groups are found through the whole system while the shorter-lived DNP groups mostly decay before even exiting the core piping. The species concentrations calculated in the standalone 1D model are also higher in magnitude than what was calculated in the coupled 2D-1D model, and the difference in magnitude is likely because of the power density and power profile differences between the models.

As mentioned previously, a pump coast-down transient was simulated using the coupled 2D-1D model and the standalone 1D model. The transient was initiated at a time of $t = 1$s, and the pump head was reduced to 20% of the nominal head over a period of 10 seconds. The transient was then continued for a total time of 400 seconds. The results from the transient simulations are shown below in Figure 4-1(a)-(f) and Figure 4-2(a)-(f).

Figure 4-1(a) shows a plot comparing the normalized reactor power over the course of the pump coast-down transient. In the beginning of the transient, both models predict similar reactor power transient responses. However, after the pump head is fully reduced to 20% of the nominal head, the standalone 1D model starts to deviate and predict lower power values than what is predicted in the coupled 2D-1D model. Although the transient reactor power is lower in the standalone 1D model, both models follow the same qualitative trend with a second power peak and finally reaching a new steady state reactor power level. The final reactor power predicted by the coupled 2D-1D model was 66.4% of the initial reactor power, and the standalone 1D model predicted a final reactor power of 63.9% of the initial reactor power. Figure 4-1(b) shows the mass flow predicted by both models, and both models predicted the same mass flow over the transient within 1% difference of each other. Figure 4-1(c), Figure 4-1(d), and Figure 4-1(e) show the core temperature increase, the predicted inlet and outlet core temperatures, and the average core temperatures, respectively. From the figures, it is shown that the temperature plots behave similarly in shape but differ in magnitude where the coupled 2D-1D model predicted a higher core ΔT and average core temperature, which is expected since the coupled 2D-1D model predicted a larger reactor power with a similar flow rate to the standalone 1D model. Lastly, Figure 4-1(f) shows the combined reactivity feedback from fuel doppler and density effects. In the beginning of the transient, both models were shown to predict the same reactivity feedback, but shortly after the pump was fully reduced to 20% head, the reactivity feedback effects started to deviate from each

other where the standalone 1D model predicted larger negative reactivity feedback than what was predicted in the coupled 2D-1D model. As the transient simulation continued toward steady state, this discrepancy carried through where the standalone 1D model predicted a combined fuel density and doppler reactivity feedback about twice as much as what was predicted in the coupled 2D-1D model. The reason the reactivity feedback effects can achieve steady state at negative reactivity values is because of the contribution from the DNP drift in the system. In the modified PKE equations, the DNP flux difference between the inlet and outlet core boundaries is also considered for the reactor power transient calculations. To give a better understanding of the effects of DNP drift on the PKE calculations, the DNP flux difference was plotted over the course of the transient. The DNP flux differences for each group are shown below in Figure 4-2(a)-(f).

As seen above in Figure 4-2(a)-(f), the DNP flux difference between the inlet and outlet core boundaries was shown to increase over the course of the transient. Oscillations in the flux differences predicted by the models are physical and the effect is due to the recirculation of the DNPs which is why the oscillations are more pronounced in the longer-lived groups than the shorter-lived groups. Although the coupled 2D-1D model predicted oscillations as well, the standalone 1D model was found to have much more prominent oscillations. This may be because the resonance time is increased in the 2D core model, and more DNP groups are allowed to decay which dampens the oscillation effects. As it related to the reactor power calculations in the PKEs, it is shown that the standalone 1D model predicts a much larger increase in the DNP fluxes than what was predicted in the coupled 2D-1D model, apart from DNP group 6. The flux difference increases in the DNP groups create a positive reactivity feedback effect with their implementation into the modified PKEs. This is the reason why the combined reactivity feedback from fuel density and doppler effects can converge to steady state at negative values because the negative feedback from fuel density and doppler effects compensates for the positive reactivity feedback created from the increase in DNP flux differences at the core inlet and outlet. As also seen in the figures, the standalone 1D model predicts larger increases in the DNP flux difference over time than what was predicted in the coupled 2D-1D model, and this is shown to agree with the fact that the standalone 1D model predicted a larger final combined reactivity feedback from fuel density and doppler effects than the coupled 2D-1D model. More work will be performed to understand the differences in the feedback effects from the DNP drift through the core.

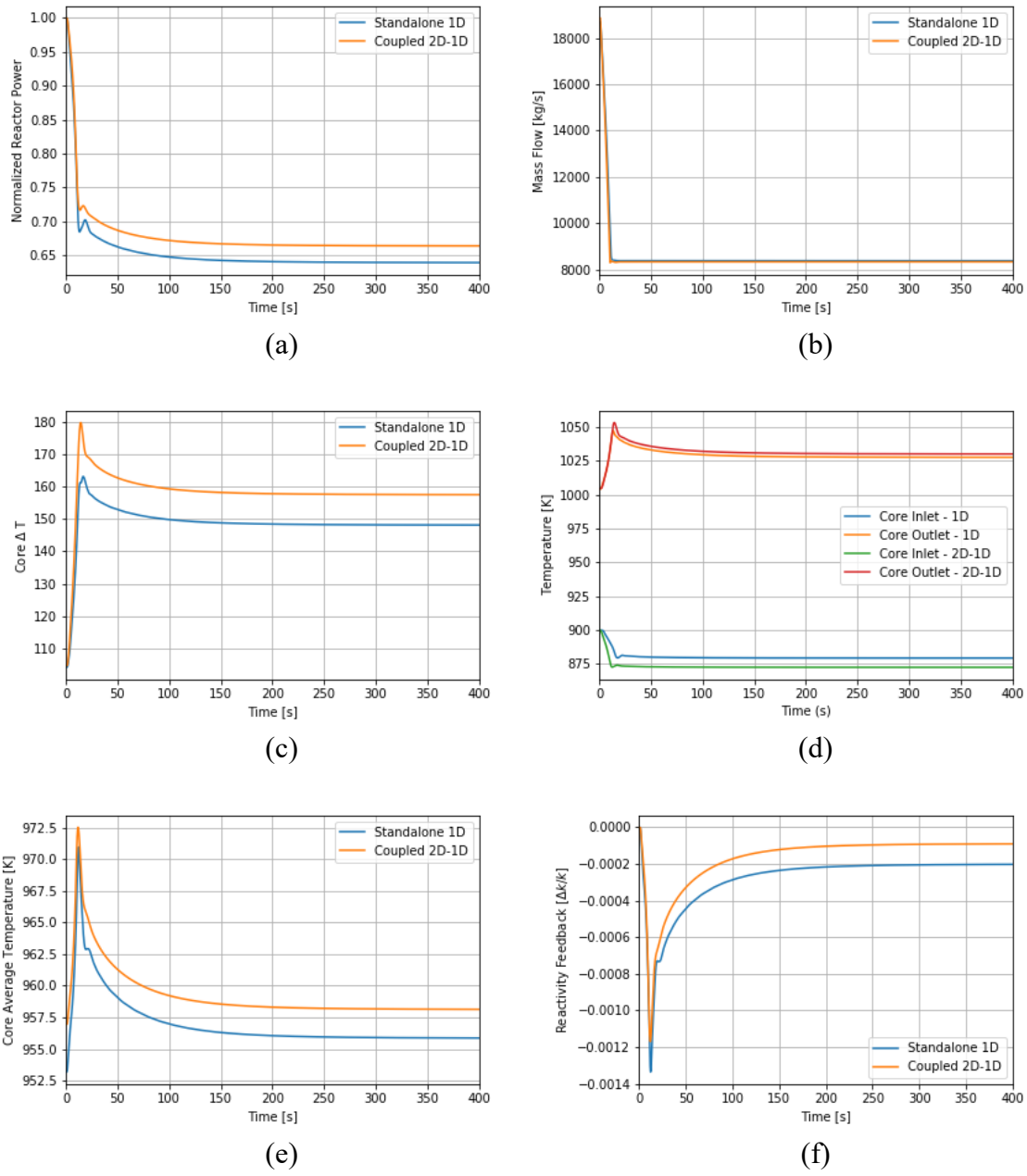

Figure 4-1. Transient simulations results showing the (a) normalized reactor power, (b) mass flow rate, (c) core temperature increase, (d) core inlet and outlet temperatures, (e) core average temperature, and the (f) combined reactivity effects from density and fuel temperature from both models.

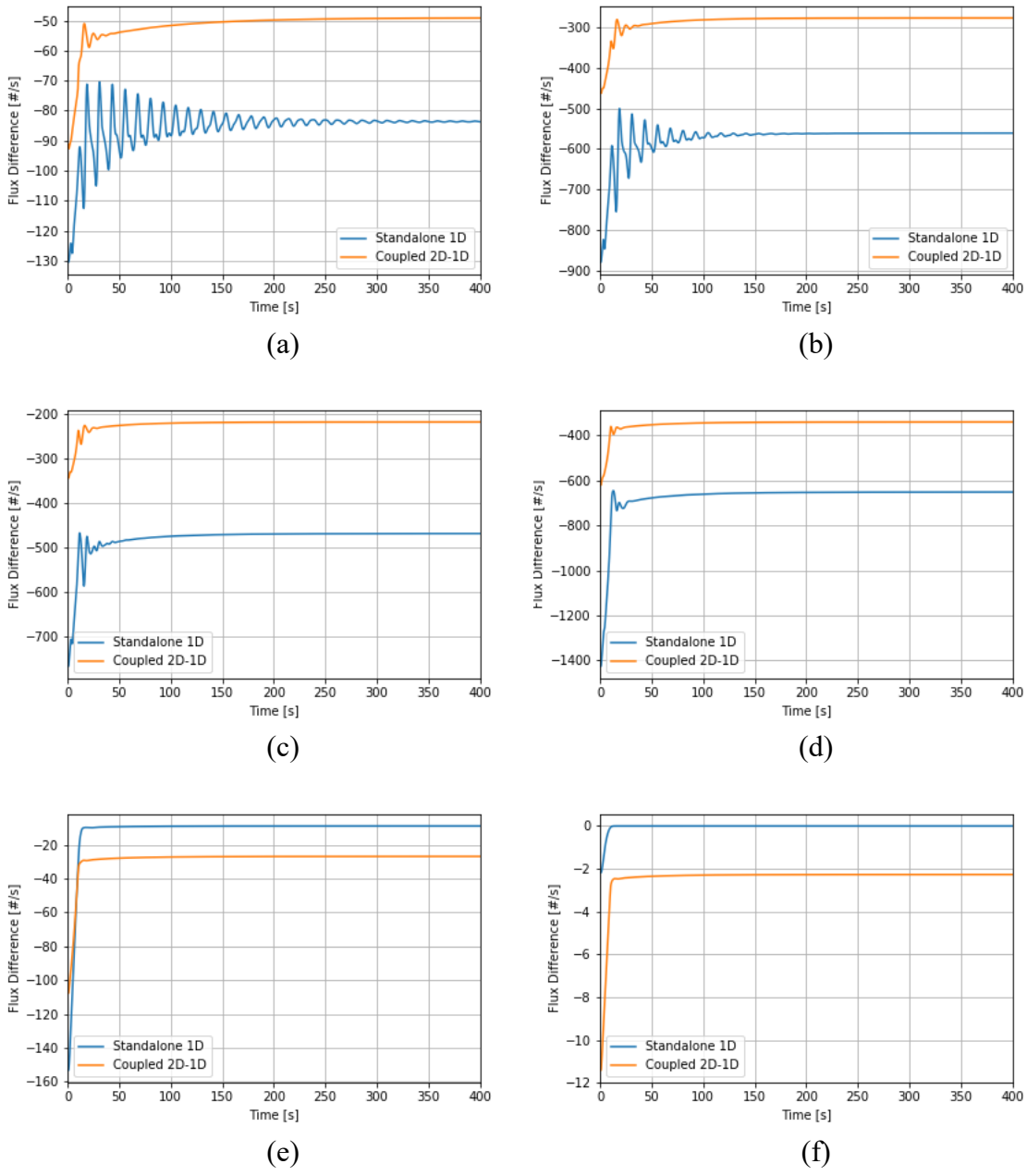

Figure 4-2. Transient results of the core inlet and outlet species flux difference for DNP group (a) 1, (b) 2, (c) 3, (d) 4, (e) 5, and (f) 6.

5 Bubble Transport Modeling in SAM

This activity focused on improving on modeling capabilities in SAM for transported gasses in MSR systems. Designs that have the fuel dissolved directly into the coolant, pose unique chemistry and corrosion challenges that must be understood, including production and removal of fission products, transmutation of isotopes, and production and deposition of noble metals. In the NEAMS program, it is intended that the MOOSE application, Mole (Lee, 2021), which calculates macroscale and mesoscale diffusion, decay, and transmutation of radionuclides as well as phase equilibrium in multi-species systems, will be used for tracking of MSR species of importance. However, Mole will need thermal-hydraulic information including velocity and interfacial area (if the species is gaseous) which can be provided by SAM once the two capabilities are coupled.

Note that species of interest in an MSR system can include both dissolved in the liquid as well as gaseous components. For example, xenon-135 is a fission gas that is produced during normal operation and must be removed because of its high thermal neutron absorption cross section, which can cause degraded economic performance of the reactor. It was observed during the operation of the MSRE facility at ORNL in the late 1960s that introducing a dispersed helium gas into the system can improve the removal efficiency of xenon from the system (Engel, 1971). A summary of the removal process and the findings in the MSRE can be found in Taylor (Taylor, 2022). Briefly put, helium cover gas that is in contact with the free salt surface in the pump bowl is entrained during normal operation of the reactor, leading to a finely dispersed field of small helium bubbles (low void of less than 1 %, typically) that are entrained in the salt. The xenon will tend to conglomerate in the helium gas which is then removed from the system for later filtration.

Note that while SAM already has a species mass transport solver, this task focused on improving on the species transport capabilities of SAM by implementing a modeling capability for non-condensable gasses. One thing that the current SAM model does not consider is the possibility of the species to travel at a different velocity than the bulk fluid velocity. Despite volume fraction of the gas being small, it is possible that there may be a discrepancy between the gas velocity and bulk velocity, which can impact the species transport solution. A drift-flux model was used to predict the relative velocity between phases in a two-phase salt/helium system. A hand-calculation was performed using this model which demonstrates that the gas velocity can vary considerably from the bulk fluid velocity, with the slip ratio between vapor and liquid being about 2.6 for MSRE conditions. Because of this, the drift-flux model was implemented into SAM to enable further testing for more complex geometries and in the future coupling of SAM and Mole. This task was supported as a Level 4 milestone and is documented in more details in (Salko, 2021).

The drift-flux model that was implemented into SAM was that proposed by Zuber and Findlay (Zuber, 1965), as shown below.

$$\overline{v_g} = C_0\langle j\rangle + \frac{\langle \alpha V_{gj}\rangle}{\langle \alpha\rangle}$$

In this equation, j is the volumetric flux of the fluid, v_g is the gas velocity that will be used to transport the species, C_0 is known as the distribution parameter, and v_{gj} is the drift velocity. The angle brackets denote the fact that an area-weighting is being used. The distribution parameter is available from empirical relations. The model of Ishii (Ishii, 1977) for bubbly flow is being used

in this case, which is expressed as a max-to-mean ratio of velocity of a single-phase flow in a tube, C_∞, which is defined as follows.

$$C_\infty = 1.393 - 0.0155 \ln\left(GD/\mu_f\right)$$

Here, G is the fluid mass flux, D is the hydraulic diameter, and μ_f is the fluid viscosity. This is used to calculate the distribution parameter, as follows.

$$C_0 = C_\infty - (C_\infty - 1)\sqrt{\frac{\rho_g}{\rho_f}}$$

The density is represented as ρ and the f and g subscripts represent liquid and gas, respectively. The drift velocity, V_{gj} was defined by Zuber for bubbly flow as follows.

$$V_{gj} = 1.53\left(\frac{\sigma g \Delta\rho}{\rho_f^2}\right)^{\frac{1}{4}}$$

Here, the fluid surface tension is σ, gravitational acceleration is g, and $\Delta\rho$ is the difference between gas and liquid density. It is noted that both the distribution parameter and the drift velocity were qualified using steam-water or air-water mixtures, and so work will be needed to qualify them for salt/gas mixtures. Considering that for MSR applications, void will be very low (i.e., less than 1 %), it is safe to assume that j is equal to the liquid velocity predicted by SAM during its regular governing equation solve.

To determine the rate of mass transport between liquid and the gas phase, Mole will need to know the interfacial area of the gas phase, which requires knowledge of the total gas volume fraction and bubble size distribution. The interfacial area can be estimated by assuming that the bubbles will have a spherical shape, which leads to the following expression for surface area per unit volume for a single bubble.

$$A_i''' = \frac{\alpha 4\pi r^2}{\frac{4}{3}\pi r^3} = \frac{3\alpha}{r}$$

Here, the numerator is the surface area of a bubble and denominator is the volume of a bubble, where r is the bubble radius. By multiplying this by the volume fraction, the total interfacial area of bubbles is obtained. Note that the volume fraction can be obtained from the drift-flux model that has been previously stated. The maximum bubble radius can be determined from the Weber number, which can be thought of as the ratio between the inertial and surface tension forces of the bubble, as shown below:

$$We = \frac{\rho v^2 l}{\sigma}$$

Considering that v will be the relative velocity between gas and liquid (obtained from the drift-flux model) and that the characteristic length, l, represent the bubble radius, this can be rearranged to provide the bubble radius:

$$r = \frac{We\sigma}{2\rho_f v_r^2}$$

The Weber number, which has previously been chosen as 10 for LWR applications (Salko, 2019), will likely be less for salt applications which has a higher surface tension. In an experimental study of helium flowing upwards in FLiNaK (Chavez, 2020), it was stated that this was between 1.59 and 4.36, so a value of 3.0 was chosen for this work. To limit bubble radius to reasonable values, an upper limit of 2 mm was enforced.

Two options have been added to the SAM input, which are valid when transported species are defined.

- "ps_use_drift_flux" is a vector input that takes a Boolean input for each species in the model. When set to True for a species, that particular species will be transported by the drift-flux model. The default value for this input, if not provided, will be False, meaning that the bulk liquid velocity will be used for species transport.
- "ps_is_gas" is a vector input that takes a Boolean input for each species defined in the model. When set to True for a species, that particular species is defined as being a gas, which prompts SAM to calculate gas properties including volume fraction and interfacial area. The default value for this input, if not provided, will be False, meaning that the species will be treated as a liquid.

To allow for Mole to obtain these new solution values and for the user to print them to output, AuxKernels were added for the calculations. The variables will be named using the declared species name (set by the user) affixed by an underscore and an identifier. Specifically, gas bubble radius can be obtained using *species*_rad, gas interfacial area by *species*_aint, gas volume fraction by *species*_void, and gas velocity by *species*_vel, where "*species*", denotes the name of the species.

To test this new feature, an unheated, horizontal oriented PBOneDFluidComponent was created. The reason for orienting the component horizontally was to eliminate the gravitational head pressure loss. The friction was also set to zero to ensure there was no pressure change throughout the component. This allows for more a better comparison of hand-calculated and SAM-calculated values. The component was 1 m long and was broken into 5 nodes. A function was used to set a constant species volumetric source term in the first node of the component with zero generation downstream of that. The inlet boundary condition was placed at the bottom of the component and included an inlet velocity of 0.213 m/s, inlet temperature of 707.15 K, and zero species concentration. The outlet boundary condition was placed at the top of the component and included an outlet pressure of 101.325 kPa. The geometry was created to be consistent with an MSRE flow channel, which had a flow area of 2.88e-4 m^2 and hydraulic diameter of 1.59e-2 m.

By using a volumetric generation source term for the species, it is ensured that the mass injection of the species is the same. It is shown that the species velocity when using the drift-flux model is 0.561 m/s compared to the salt velocity of 0.213 m/s. Because of this, the predicted volume fraction is much lower with the drift-flux model enabled, as shown in Figure 5-1. Note

that the volume fraction is very low, but this is the range of void that was observed in the MSRE experiment. Figure 5-2 shows the difference in gas species interfacial area between the two models; however, recall that bubble radius will be set to the upper limit of 2 mm for the base model, as phase slip is not calculated. Note also that the bubble radius, interfacial area, volume fraction, and drift velocity were manually calculated for the problem conditions and were found to be in good agreement with the SAM predicted values.

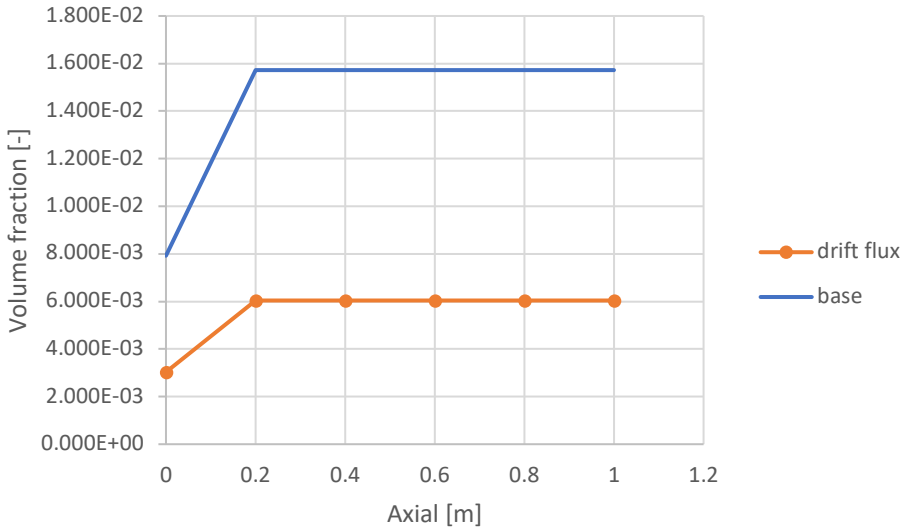

Figure 5-1: Axial void distribution using the base and drift-flux models in SAM

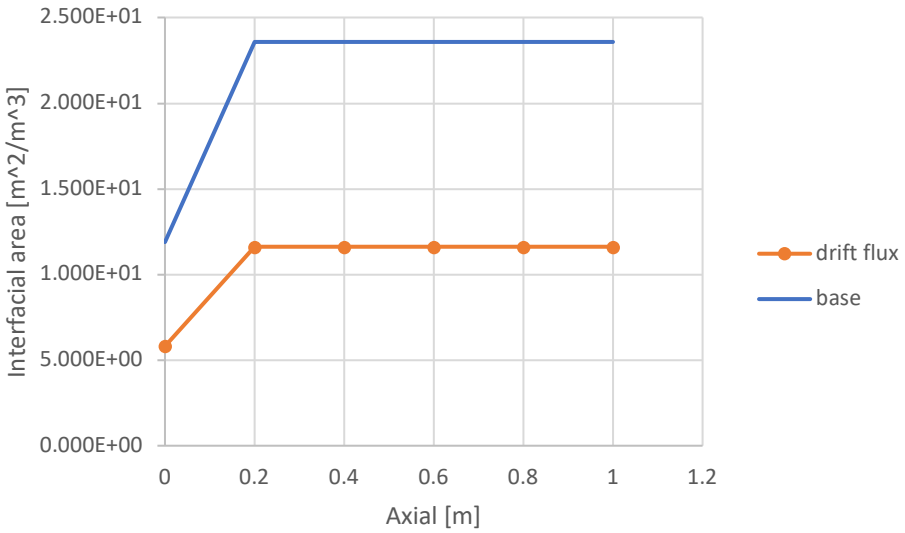

Figure 5-2: Interfacial area distribution using the base and drift-flux model for gas species transport

In addition to the unheated test, two additional cases were run that included more complex geometry. One case had three *PBOneDFluidComponent* objects connected by a *PBBranch* junction component with flow going into the bottom of one pipe and splitting into the two pipes above via the junction. A second case included two *PBOneDFluidComponent* objects connected by a *PBSingleJunction* component with one pipe in the vertical orientation and the other in the

horizontal configuration. In both of these unheated cases, it was verified that injecting a species at the inlet led to a uniform species distribution through the entire geometry and that the species was properly transferred from one component to another.

In future work, it is planned to increase the complexity of the geometry of test cases, building up to MSR loop geometry (likely MSRE model geometry). Furthermore, support will be provided for the coupling of the SAM and Mole for testing of the new models in a multi-physics simulation. Finally, several improvements will be needed to the thermophysical properties that are being used. First, it was assumed that the gas is always helium and properties were set accordingly. This assumption will need to be corrected by taking gas equation of state as input from the user. Second, salt properties needed for the calculations were not always available and will need to be revisited. It is intended that integration of the Saline MSR property database (Henderson, 2021) will improve on fluid properties in the calculation.

Acknowledgement

This work is supported by the U.S. DOE Office of Nuclear Energy's Nuclear Energy Advanced Modeling and Simulation program, under Contract No. DE-AC02-06CH11357. The ORNL portion of this work is supported by the U.S. Department of Energy, under Contract DE-AC05-00OR22725.

The SAM code development has been funded by multiple sources including several DOE programs (including NEAMS, GAIN, TCF, FOA), Argonne LDRD, and the U.S. Nuclear Regulatory Commission. The SAM development, demonstration, and validation for MSR were greatly aided by additional efforts and inputs from many colleagues and collaborators, especially Ling Zou, Thanh Hua, Bo Feng, and Elia Merzari at Argonne National Laboratory.

Reference:

[1] R. Hu et al., SAM Theory Manual, Argonne National Laboratory, ANL/NE-17/4 Rev. 1, February 2021.

[2] J. Serp et al., The molten salt reactor (MSR) in generation IV: Overview and perspectives, Progress in Nuclear Energy, 77, pp. 308-319, 2014.

[3] H. Rouch et al., Preliminary thermal-hydraulics core design of the Molten Salt Fast Reactor (MSFR), Annals of Nuclear Energy, 64, pp. 449-456, 2014.

[4] E.E. Pettersen, Coupled multi-physics simulations of the Molten Salt Fast Reactor using coarse-mesh thermal-hydraulics and spatial neutronics, Master Thesis, Universite Paris-Saclay, 2016.

[5] Robertson, R. C. (1965). MSRE design and operations report. Part I. Description of reactor design. Technical Report: ORNL-TM-2316, Oak Ridge National Laboratory.

[6] Beall, S. E., Haubenreich, P. N., Lindauer, R. B., & Tallackson, J. R. (1964). MSRE Design and Operations Report. Part V. Reactor Safety Analysis Report. Technical Report: ORNL-TM-732, Oak Ridge National Laboratory.

[7] Cantor, S. (1968). Physical Properties of Molten-Salt Reactor Fuel, Coolant, and Flush Salts. Technical Report: ORNL-TM-2316, Oak Ridge National Laboratory. https://doi.org/10.2172/4492893

[8] Fang, J., Hu, R., Gorman, M., Zou, L., Hu, G., & Hua, T. (2020). SAM Enhancements and Model Developments for Molten-Salt-Fueled Reactors. Technical Report: ANL/NSE-20/66, Argonne National Laboratory.

[9] Guymon, R. H. (1973). MSRE systems and components performance. Technical Report: ORNL-TM-2316, Oak Ridge National Laboratory.

[10] K. O. Lee, Z. Taylor, and B. Collins. Implementation of decay and liquid-gas mass transfer to enhance mass accountancy capabilities in mole. Technical Report ORNL/TM-2021/2161, Oak Ridge National Laboratory, 2021.

[11] J. Engel and R. Steffy. Xenon behaviour in the molten salt reactor experiment. Technical Report ORNL-TM-3464, Oak Ridge National Laboratory, 1971

[12] Zack Taylor, Robert Salko, Aaron M. Graham, Benjamin S. Collins, and G. Ivan Maldonado. Implementation of two-phase gas transport into vera for molten salt reactor analysis. Annals of NuclearEnergy, 165:108672, 2022. ISSN 0306-4549. doi: https://doi.org/10.1016/j.anucene.2021.108672. URL: https://www.sciencedirect.com/science/article/pii/S030645492100548X.

[13] Robert Salko, Travis Mui, Rui Hu, and Elia Merzari. Implementation of a Drift-Flux Model in SAM for Modeling of Passively Transported Gas in Molten Salt Reactors. Technical Report ORNL-TM-2021/2241.

[14] R. Salko, M. Avramova, A. Wysocki, A. Toptan, J. Hu, N. Porter, T. Blyth, C. Dances, A. Gomez,C. Jernigan, J. Kelly, and A. Abarca. CTF Theory Manual. Consortium for Advanced Simulation of Light Water Reactors, 2019.

[15] D. E. Chavez. Flow visualization of two-phase flow in molten-salt: Helium bubbling in lithiumfluoride-sodium fluoride-potassium fluoride (lif-na-kf). Master's thesis, Texas A&M University, 2020.URL http://hdl.handle.net/1969.1/192215.

[16] S. Henderson, C. Agca, J. McMurray, and R. Lefebvre. Saline: An API for Thermophysical Properties. Technical Report ORNL/TM-2021/2239, Oak Ridge National Laboratory, 2021.

Nuclear Science and Engineering Division
Argonne National Laboratory
9700 South Cass Avenue, Bldg. 208
Argonne, IL 60439

www.anl.gov

Argonne National Laboratory is a U.S. Department of Energy laboratory managed by UChicago Argonne, LLC